Journal of Glaciology, Vol. 27, No. 95, 1981

AN ELECTRONIC REMOTE SNOW-DRIFT GAUGE

By H. GUBLER

(Eidg. Institut für Schnee- und Lawinenforschung, 7260 Weissfluhjoch/Davos, Switzerland)

ABSTRACT. Snow transportation by wind in potential avalanche fracture zones is a very important parameter for avalanche forecasts. A special battery-powered photoelectric sensor has been developed by the Eidg. Institut für Schnee- und Lawinenforschung, Weissfluhjoch/Davos. The output pulse rate is proportional to the mass flux (units of kg m^{-2} s^{-1}). Drift particles larger than 50 μm in diameter are classified according to their volumes in five classes. The accuracy of the flux measurement is ±50% and is limited by physical factors and not by the apparatus.

RÉSUMÉ. *Un sonde électronique de mesure de la neige soufflée.* Les accumulations de neige soufflée dans les zones potentielles de décrochement d'avalanches sont également grandement déterminantes pour les prévisions d'avalanches. Pour enregistrer le flux des masses qui passent au-dessus d'une crête, un sensor spécial, alimenté par des batteries, a été développé à l'Institut Federale pour l'Étude de la Neige et des Avalanches, Weissfluhjoch/Davos. La fréquence des pulsations provenant de l'appareil est proportionnelle au flux des masses (kg m^{-2} s^{-1}). Les particules de neige ayant un diamètre supérieur à 50 μm sont réparties en 5 classes selon leur volume. L'exactitude de mesure du flux est de ±50%; elle est limitée non pas par le capteur, mais par la méthode de mesure.

ZUSAMMENFASSUNG. *Ein elektronisches Gerät zur Messung der Schneedrift.* Schneeverfrachtungen in potentielle Lawinenanrisszonen sind für Lawinenprognosen wesentlich mitbestimmend. Zur Registrierung des Massenflusses über einen Kamm wurde am Eidg. Institut für Schnee- und Lawinenforschung, Weissfluhjoch/Davos, ein spezieller batterie-betriebener Sensor entwickelt. Die Ausgangspulsrate des Gerätes ist proportional dem Massenfluss (kg m^{-2} s^{-1}). Schneepartikel mit Durchmessern grösser als 50 μm werden aufgrund ihres Volumens in 5 Klassen eingeteilt. Die Genauigkeit der Flussmessung beträgt ±50% und wird durch die Messmethode und nicht durch den Sensor eingeschränkt.

INTRODUCTION

Blowing snow is a very important parameter for modelling the snow stratification and for avalanche forecasting. Several attempts have been made to measure the mass flux, visibility, and particle-size distributions as a function of wind velocity, height over the snow surface, and weather conditions. Precision measurements have been made by Budd (1966), Mellor ([1960]), Föhn (1980), and personal communication from W. Pope, with rocket drift gauges. Beside these purely mechanical measurements various sensors were developed to measure blowing snow by photoelectric metering (Landon-Smith and Woodberry, 1965; Wishart, 1965; Rogers, 1968; Schmidt, 1977). Many of these systems are not designed for remote operation with low power consumptions or do not have outputs proportional to mass flux. For these reasons we decided to build and test a new, simple, inexpensive flux meter.

SYSTEM REQUIREMENTS

Measured parameter: point measurement of the mean horizontal mass flux over a ridge.

Accuracy: ±50%, independent of particle size distribution, wind speed, and temperature.

Dynamic range: 0.1–100 g m^{-2} s^{-1}.

Power requirements: suitable for remote, battery-operated or solar-powered weather stations.

Minimal sampling period: ⩽30 min depending on available power.

Output signal: analogue or digital signal proportional to the mean flux during the sampling period.

The system described herein meets all the requirements listed above except during conditions of strong precipitation-induced blowing snow.

THEORETICAL CONSIDERATIONS FOR THE DESIGN

One of the most important design parameters is determined by the distribution of the mass contribution as a function of the particle size for typical particle-size distributions. Preliminary results for Alpine blowing snow (personal communication from M. Pope) show that significant mass contribution starts for particle diameters larger than 100 μm and decreases again to insignificant values for particle diameters larger than about 800 μm. This size range corresponds to a volume or mass range of 1 to 512. It is important to notice that small changes of the percentage of large particles in the particle-size distribution cause significant changes of the mass flux. The shapes of the particle-size distributions depend on snow-surface, wind, and precipitation conditions. For these reasons we decided to design a flux meter which at least roughly classifies the particle masses to get results independent of size distribution. Unfortunately photoelectric metering allows only a classification according to the projected area of the particles instead to their volumes or masses. The mean masses have to be calculated from the measured projected areas. Figure 1 shows that for identical projected mean areas of a

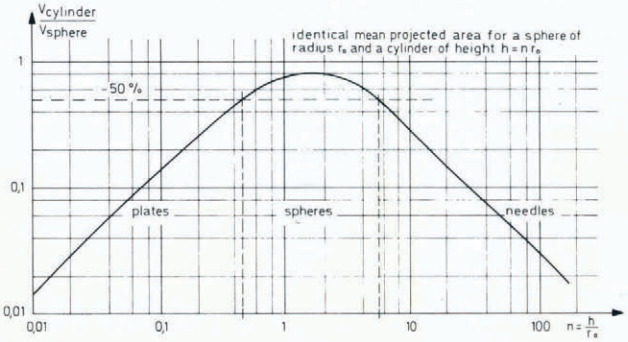

Fig. 1. Ratio of the volumes of a cylinder and a sphere (radius r_0) with identical mean projected areas as a function of the height of the cylinder $h = nr_0$.

sphere of radius r_0 and a cylinder of height $h = nr_0$, the corresponding volumes may differ by about two orders of magnitude. Considering spheres as the mean particle shape causes an overestimation of the real flux. The evaluation of particle shapes by Pope (in press) shows that for blowing snow in the absence of precipitation the particles are almost spherical (ratio of length of axis of inertia less than about three). Blowing snow during precipitation contains plates, fractured dendrites, needles, or even aggregates of crystals. To get some idea on the contribution of the horizontal mass flux from precipitation alone we may start with a vertical precipitation flux of 1 g m^{-2} s^{-1} (vertical velocity of the crystals 0.5 m s^{-1}, accumulation 0.05 m of new snow per hour). For a mean wind velocity of 15 m s^{-1} the precipitation-induced horizontal mass flux reaches 30 g m^{-2} s^{-1}. This flux corresponds to the highest measured mean fluxes (0.5 m above ground) at similar wind velocities without precipitation. This estimation shows that the photoelectrically measured total fluxes (during precipitation), assuming spherical particles, may significantly exceed the real mass fluxes.

The drift flux decreases rapidly with increasing height above the snow surface. To get consistent drift data at constant height above the snow surface (independently of the total snow depth) the photoelectric sensor is mounted under a wind-roof (0.5 m above ground), located on a ridge. The wind-roof is designed to prevent significant snow accumulation below the gauge during conditions of blowing snow. The concentration factor for the wind-roof is chosen as small as possible to decrease the disturbance of the natural wind profile.

https://doi.org/10.3189/S0022143000011321 Published online by Cambridge University Press

The maximum possible particle flux is also an important design parameter. The maximum horizontal mass flux under conditions of strong drift and precipitation (accumulation 0.1 m new snow per hour corresponding to 3 g m^{-2} s^{-1}, mean vertical particle speed 0.5 m s^{-1}, horizontal 25 m s^{-1}, gust factor 1.6) amounts to about 600 g m^{-2} s^{-1}. For a mean particle diameter of 200 μm the corresponding maximum particle flux reaches 5×10^8 m^{-2} s^{-1}.

Fundamentals of the design

The drifting snow particles cross a 0.02 m long infrared light beam with a rectangular cross-section 1 mm high and 0.5 mm wide (Fig. 2). A highly sensitive photodiode detects the shadows of the particles. The corresponding voltage pulse height is proportional to the

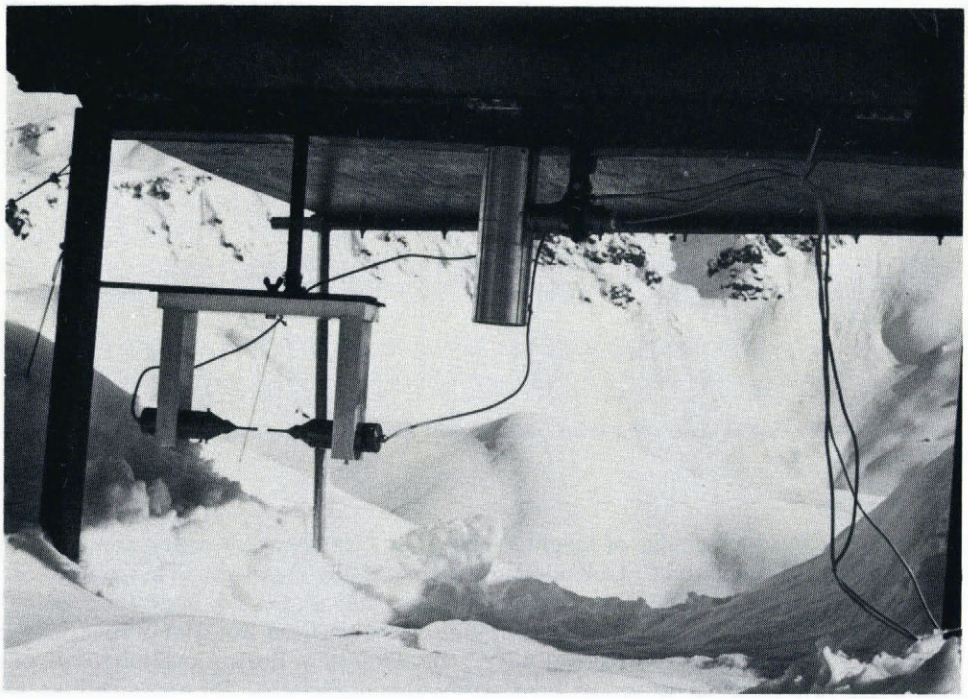

Fig. 2. The flux meter in position.

projected area of a particle crossing the light beam assuming that the particle dimensions are smaller or equal to the width of the light beam. All pulses higher than a certain lowest level are resolved into five classes. To get a good approximation for the real flux and a simple electronic design, the classes are defined according to the following rules: (1) Each class corresponds to a certain length of pulse train. The number of pulses in the train is proportional to the volume of a mean size particle of the class. (2) The discriminator levels separating the five classes have to be set proportional to the corresponding particle areas. The relative classification chosen is given in Table I.

The electronic design is described in the Appendix.

https://doi.org/10.3189/S0022143000011321 Published online by Cambridge University Press

TABLE I. PARTICLE CLASSIFICATION RULES

Volume proportional to pulse train length	*Relative particle diameters for spheres*	*Relative levels of the discriminators determining the class boundaries*	*Corresponding relative particle diameters*
		D1 1	1
1	1		1.42
		D2 3.35	1.82
4	1.59		2.25
		D3 6.44	2.54
8	2		2.83
		D4 10.23	3.12
16	2.52		3.57
		D5 21.29	4.61
64	4		5.66
			(6.71)*

* Theoretical upper limit of the uppermost class; no electronic limitation.

POWER REQUIREMENTS

The sensor is designed for battery operation. The power requirements depend on the sampling rate. If n is the number of samples per minute, the mean supply currents are: +12 V, $(2+3n)$ mA; −12 V, $1n$ mA. For a six months operating period, the following battery specifications are required: +12 V, $5(2+3n)$ A h; −12 V, $5n$ A h. In our case, the flux meter is integrated in a remote station, powered by solar cells. The data are transmitted by radio to the Institut.

LIMITS OF ACCURACY DETERMINED BY THE DESIGN

Figure 3 shows approximate fits to typical particle-size distributions $f(d)$ (where d is the particle diameter) measured by M. Pope (personal communication in 1979). The data may be very roughly fitted by the sum of two ln-normal distributions (dashed curves). The distributions show long tails toward large particle sizes. In the plots the mass contribution curves $d^3f(d)$ are calculated from the size distributions $f(d)$. The histogram overlay corresponds to the classification. The bars near the tops of the columns show the representative particle volumes of the classes. These values have to be compared with the real means of the classes given by the histogram. The maximum deviation amounts to 13%, the weighted mean deviations for the two distributions are 5% and 1%.

If the particle-size distributions are cut at a particle diameter of 1 mm, the off-range mass contributions are: example 1: 4%; example 2: 20%. Because the sensor registers all particles with diameters larger than 500 μm as 500 μm particles, the real deviations are considerably smaller.

The slit height of only 1 mm causes an additional restriction to the precision of the flux meter. Particles crossing the boundary of the light beam are measured with too small a mass. On the average, the recorded volumes of the particle section in the beam amounts only to 0.735 of the effective section volume (Fig. 4). This number corresponds to the highest possible error. For the particle-size distribution given in Figure 3, the erroneous mean systematic mass reduction amounts to 10%–15%.

The maximum slit height is limited by the maximum possible particle counting frequency of the system and by the light-beam optics. The light intensity has to be homogenous to within ±5% over the beam cross-section. The beam shape is defined by one limiting slit mounted

https://doi.org/10.3189/S0022143000011321 Published online by Cambridge University Press

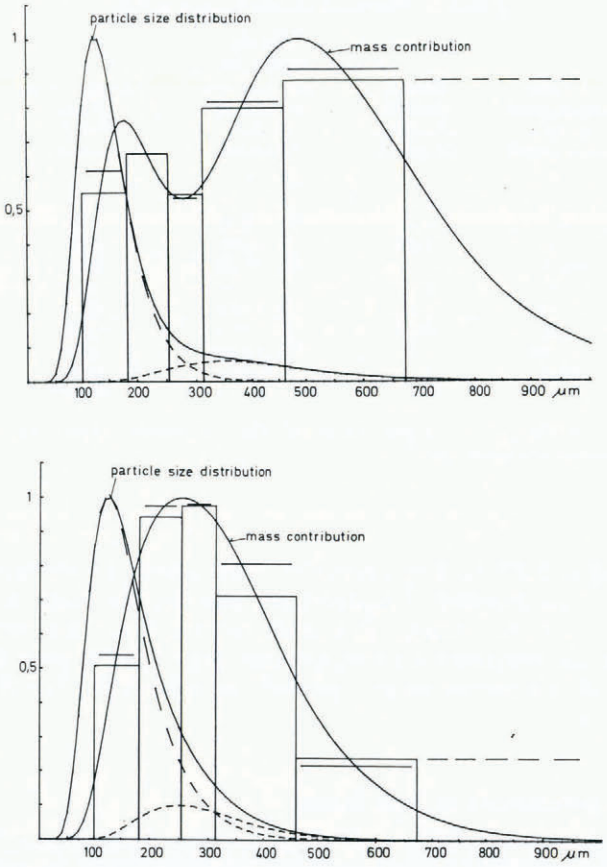

Fig. 3. Approximate fits to typical particle-size distribution $f(d)$. The histogram corresponds to the chosen classification. The bars near the tops of the columns show the representative particle volumes of the classes. The shape of the tail of the particle-size distribution towards high particle diameters depends strongly on snow-surface and wind conditions.

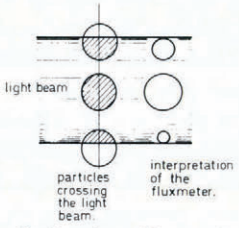

Fig. 4. Diagram to show that the mass contribution of particles crossing the boundary of the light beam is too small.

in front of the light source. The light from the high-directivity light-emitting diode is collimated and refocussed to the photodiode by lenses (Fig. 5). The maximum possible detectable particle frequency (particles with volumes corresponding to class 2) is limited by the electronics to 6.5 kHz. The sensitive counting area amounts to 2×10^{-5} m^2. Particle fluxes up to about 3×10^8 m^{-2} s^{-1}, corresponding almost to the maximum expectable particle flux during strong precipitation, are treated correctly.

https://doi.org/10.3189/S0022143000011321 Published online by Cambridge University Press

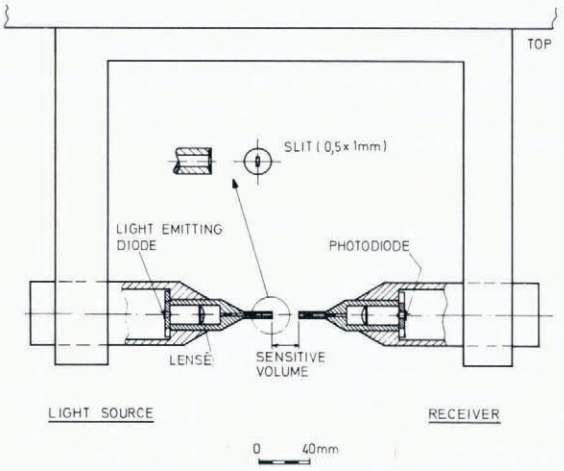

Fig. 5. Light source.

Calibration

The lowest possible setting of the discriminator D1 corresponds to a particle diameter of about 50 μm. Knowing the approximate distribution of the mass contribution (Figs 3 and 4) we set D1 to 100 μm. The sensor is calibrated by spinning a wire (diameter 50 μm) through the light beam. The battery-operated motor equipped with radial test wires simulates particle speeds between 5 m s^{-1} and 35 m s^{-1} and particle frequencies from <10 Hz up to >1 000 Hz. The spinning wire corresponds to a particle with a diameter of 253 μm. This value corresponds to the D3 discriminator level (Table I). This fact allows for a very accurate adjustment of the total amplification (Fig. 6, absolute particle size). The linearity between the projected

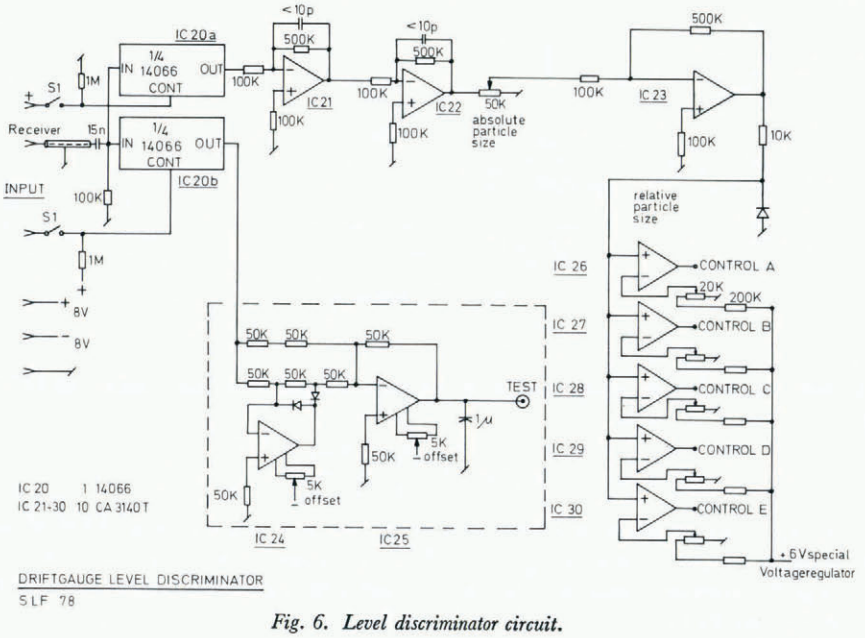

Fig. 6. Level discriminator circuit.

https://doi.org/10.3189/S0022143000011321 Published online by Cambridge University Press

area and the resulting analogue pulse height was tested by using wire of different diameters, spun through the light beam parallel or perpendicular to the slit. Schmidt (1977) showed that snow particles behave like sand particles or the test wire (i.e. opaque objects). The switch S1 (Fig. 7) is used to test the stability of the light source and of the preamplifier, as well as of the mechanical adjustment of the sensor, by measuring a d.c. voltage at the test output.

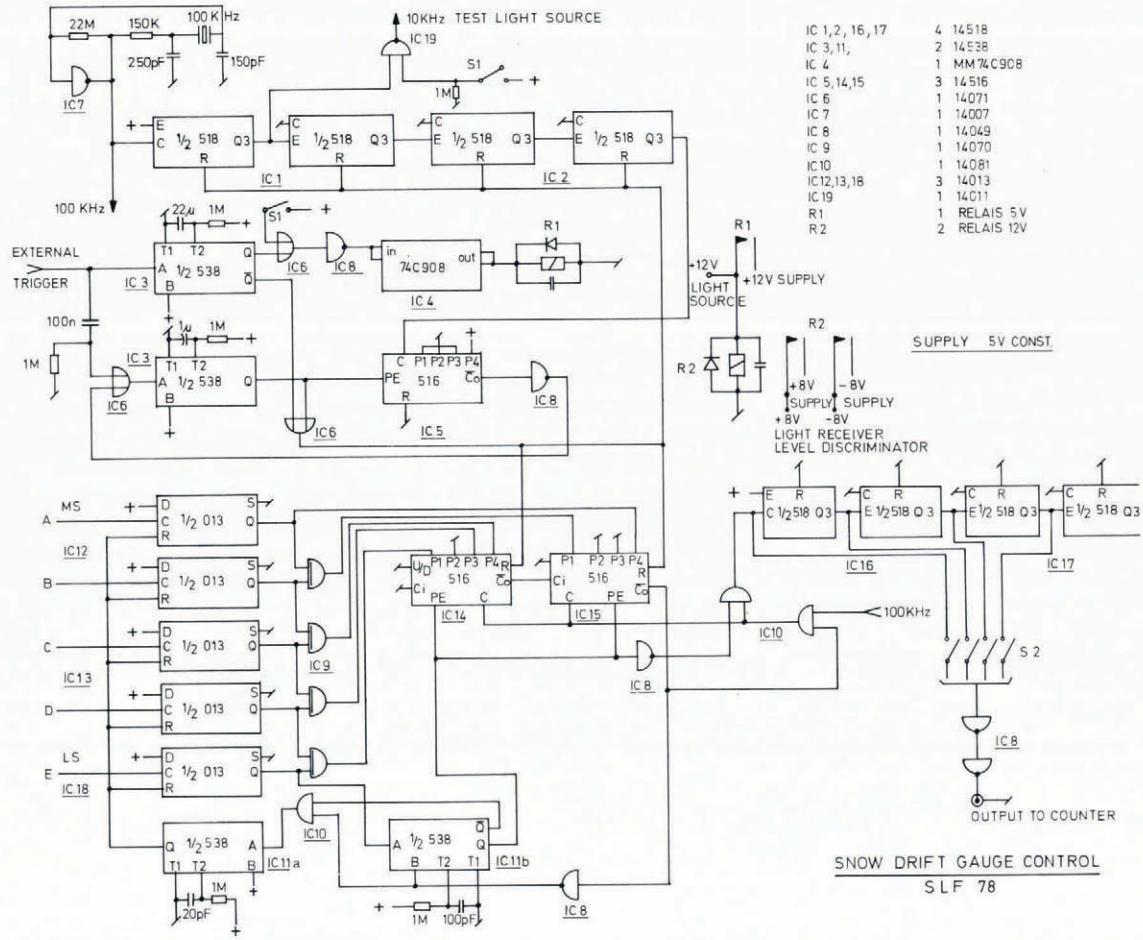

Fig. 7. Control circuit.

The mean mass flux ϕ in units of kg m^{-2} s^{-1} as a function of the total count C is given by Equation (1).

$$\phi = C \frac{(1.42 d_1/2)^3 \tfrac{4}{3} \pi 918}{T n \tau F}, \qquad (1)$$

where T is the time between two counter outputs in minutes, n the number of samples per minute, τ the duration of one sample (0.8 s), F the sensitive area (2×10^{-5} m^2), C the total count during the period T, and d_1 the particle diameter corresponding to the lowest discriminator level in metres.

https://doi.org/10.3189/S0022143000011321 Published online by Cambridge University Press

Simultaneous measurements with different types of snow flux gauges to get additional field calibrations have not yet been performed for different reasons; the only existing and laboratory-calibrated photoelectric system (Schmidt, 1977) was not available and has the same intrinsic inaccuracy related to the changing grain shapes. A Mellor-type snow trap is now used by Föhn (1980), but those measurements were not performed at the same location. Nevertheless the correspondance of the results is satisfactory.

Summary of the systematic and statistical errors

The systematic errors depend on the particle-shape distribution, the particle-size distribution, and the boundary effects. Estimates of the errors are listed in Table II.

Table II. Estimates of the systematic errors

Source of the error	*Relative deviation*
(1) Particle shape not spherical:	
No precipitation	0 to +30% (Fig. 1)
Strong precipitation	Not known (Fig. 1)*
(2) Particle-size distribution (Figs 3 and 4)	−19% to +1%
(3) Boundary effects	−15% to −10%
(4) Light intensity changes as a function of temperature	−5% to +5%
Limits of systematic errors	−39% to +26%

* During strong precipitation and with low wind speeds the particles are no longer mainly convex and often have ratios of lengths of axes of inertia larger than 3.

Source (1) of error (Table II) is inherent in the method and cannot be decreased by technical improvements.

The sources of possible statistical errors are the sampling rate and drift fluctuations.

The probability of a drift particle crossing into the sensitive area is very low. These events may be considered to be distributed according to a Poisson distribution.

To calculate the standard deviation, the total particle count instead of the recorded total mass-proportional count must be estimated.

The mass-proportional count C (Equation (1)) is equal to

$$C = \frac{\phi T n}{B}, \tag{2}$$

$$C = \sum_{i=1}^{5} C_i = \sum_{i=1}^{5} M_i p_i = \sum_{i=1}^{5} n_i C,$$

$$p_i = \frac{n_i}{M_i} C = \sigma_i^2, \tag{3}$$

where C_i is the count in class i, B the design constant defined by Equation (1), M_i the pulse train length corresponding to the ith class, n_i the relative portion of the ith class to the total mass contribution, p_i the particle count in class i, σ_i the standard deviation for class i, and σ the standard deviation for the flux.

The quantity D given by the equation

$$D^2 = \sum_{i=1}^{5} \frac{n_i}{M_i}$$

depends on the mass contribution curve. The values for the two distributions given in

https://doi.org/10.3189/S0022143000011321 Published online by Cambridge University Press

Figures 3 and 4 are $D_1 = 0.80$, $D_2 = 0.86$. For the relative error of the flux measurement we get

$$r_\phi = \frac{\sigma}{CD^2} = \frac{1}{D\sqrt{C}} = \frac{1}{D}\frac{\sqrt{B}}{(\phi Tn)^{\frac{1}{2}}}. \quad (4)$$

In our case $\sqrt{B}$ is equal to 9.27×10^{-3}. For $n = 1$ min^{-1}, $T = 30$ min, $\phi = 1$ g m^{-2} s^{-1}, we get $r_\phi = 7\%$, for a flux of 0.1 g m^{-2} s^{-1} about 21%.

This estimate shows that even for very low sampling rates this contribution to the total error is insignificant compared with the possible systematic errors.

The last error contribution is determined by the gustiness of the wind. Cramer (1960) gives the following relationship for the standard deviation σ_v of wind fluctuations when the mean wind speed is $\bar{v}$:

$$\sigma_v = 0.25\bar{v}. \quad (5)$$

If the wind speed is sampled n times per minute during time T, the resulting standard deviation of the measured mean is

$$\sigma_{\bar{v}} = \frac{0.25\bar{v}}{(Tn)^{\frac{1}{2}}}. \quad (6)$$

The transportation of snow mass is roughly proportional to the third power of the actual wind speed. The resulting relative standard deviation of the flux is

$$r_\phi = 0.75\frac{1}{(Tn)^{\frac{1}{2}}}. \quad (7)$$

The error contribution is again less than 10%.

In retrospect, the contributions of the statistical errors for mean drift fluxes of some g m^{-2} s^{-1} are less than 50% of the possible systematic errors. If the contribution from precipitation is not significant, the accuracy of a flux measurement is in the range of $\pm 50\%$.

Measurements and results

The sensor has been in operation as part of the "Gaudergrat" remote station for five months. After some initial electronic and calibration problems had been solved, the flux gauge produced good data for three months. The data were transmitted to the Institut on Weissfluhjoch by radio where they have been analysed on line by a Hewlett Packard desk computer 9815. A typical plot of the mean flux over the "Gaudergrat" crest recorded 0.5 m above ground under the wind-roof together with the corresponding mean wind speed (recorded 3 m above ground) is shown in the preceding paper (Gubler, 1981, fig. 11). The system allows the investigation of the dependence of the mean mass flux on the development of the snow surface conditions (erodibility of the surface) and on the mean wind speed as well as the effect of low to medium precipitation. The given example includes a south-east wind situation with no precipitation and low erodibility, resulting in low fluxes even at high mean wind speeds, followed by a north-west wind situation with low to medium precipitation increasing the erodibility and causing precipitation-induced flux, resulting in significantly higher fluxes at comparably low mean wind speeds. Integral representations of the total flux across the crest at a given height above the snow surface are given by Gubler (1980). These types of calculations allow an estimation of the loading and unloading of potential fracture zones of avalanches under blowing-snow conditions. This is a very important mechanism in determining the danger of avalanches. Investigations allowing the computation of the total flux over a crest from single measurements of the flux and the wind speed at given heights above the snow surface are put forward by Föhn (1980).

MS. received 29 May 1979 and in revised form 14 September 1979

APPENDIX

Electronic set-up

Light source receiver (Fig. A1)

The high-directivity light source is operated by a stabilized voltage supply. Stability could be slightly improved by replacing the stabilized voltage source by a stabilized current source. To be able to modulate the light source for calibration purposes, the supply voltage may be turned on and off by an analogue switch (IC32). The light receiver consists of a low-noise photodiode followed by a three-stage voltage amplifier (IC35–IC37).

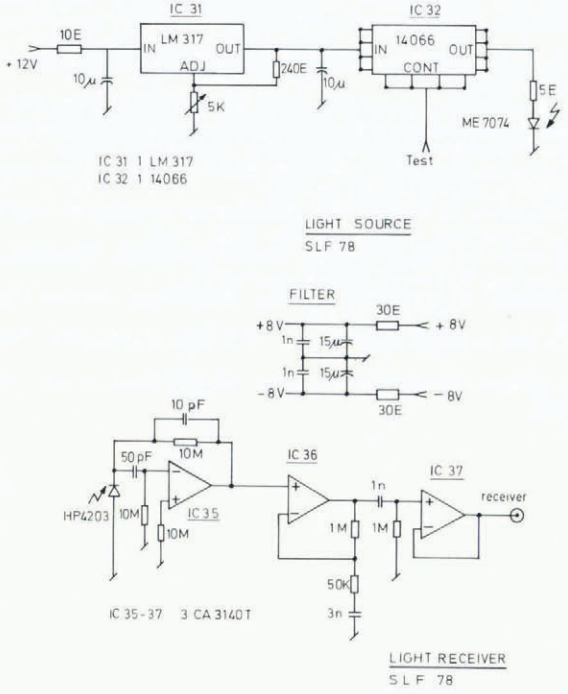

Fig. A1. Electronic circuit diagrams of the light source and receiver.

Discriminator circuit (Fig. 6)

The output signal from the receiver is either connected (IC20) to a precision full-wave rectifier (IC24, IC25) for calibration purposes or to a three-stage variable (absolute particle size) post-amplifier (IC21–IC23) followed by the five level discriminators (IC26–IC30). The band widths of the pre-amplifiers and the post-amplifiers are about 2–70 kHz. The lower limit is determined by low-speed particles (drift velocity 5 m s^{-1}, slit width 5×10^{-4} m). The high limit is given by small particles having a high velocity (drift velocity 50 m s^{-1}, particle diameter 10^{-4} m). The discriminator levels are calibrated by means of a special voltage reference (relative particle sizes).

Control unit (Fig. 7)

The timing circuit (IC3–IC6) activates the system for 0.8 s each time an external trigger pulse fires the one-shot IC3. The settling time for the analogue electronics and the light source is fixed to 1 s (IC3). The circuits are turned on by the relays R1, R2. The output frequency of the 100 kHz quartz clock (IC7) is divided down to 10 kHz and 1 Hz (IC1, IC2). The 100 kHz are fed to the down-counters IC14, IC15 (frequency in the pulse trains), the 10 kHz source is used to modulate the light source for intensity calibrations and mechanical adjustments (IC19, S1). The 1 kHz output is fed to the down-counter IC5 which determines the time interval of one measurement. A measuring cycle is started by clearing the resets of the dividers IC1, IC2 and of the down-counters IC14, IC15. The outputs of the level discriminators are connected to the flip-flops IC12, IC13, IC18. Any pulse from the level discriminators arriving at the flip-flops before the reset is cleared by the timing circuit only causes a reset of the flip-flops 100 μs later (IC11b, IC11a). Pulses arriving after the reset is cleared set the flip-flop according to the original pulse height (projected particle area) and simultaneously fire the one-shot

https://doi.org/10.3189/S0022143000011321 Published online by Cambridge University Press

IC11b. IC11b pre-sets the down-counters IC14, IC15. The most significant flip-flop which is set determines the pre-set (IC9). 100 μs later, even the slowest particle is now inside the light beam, the analogue pulse has reached its maximum, the down-counters start to count down to zero. The counting frequency is 100 kHz. During the count-down the 100 kHz pulses are fed to a scaler IC16, IC17 by IC10, IC8. If the down-counter reaches zero, the 100 kHz source is turned off (IC10), the flip-flops are reset (IC11a) and a new particle can be analysed.

The scaler output may be connected to a counter. The total count over a certain time period is proportional to the mean mass flux during this period.

REFERENCES

Budd, W. F. 1966. The Byrd snow drift project: outline and basic results. (*In* Rubin, M. J., *ed. Studies in Antarctic meteorology*. Washington, D.C., American Geophysical Union, p. 71–134. (Antarctic Research Series, Vol. 9.))

Cramer, H. E. 1960. Use of power spectra and scales of turbulence in estimating wind loads. *Meteorological Monographs*, Vol. 4, No. 22, p. 12–18.

Föhn, P. M. B. 1980. Snow transport over mountain crests. *Journal of Glaciology*, Vol. 26, No. 94, p. 469–80.

Gubler, H. 1980. Simultaneous measurements of stability indices and characteristic parameters describing the snow cover and the weather in fracture zones of avalanches. *Journal of Glaciology*, Vol. 26, No. 94, p. 65–74.

Gubler, H. 1981. An inexpensive remote snow-depth gauge based on ultrasonic wave reflection from the snow surface. *Journal of Glaciology*, Vol. 27, No. 95, p. 157–63.

Landon-Smith, I. H., *and* Woodberry, B. 1965. The photoelectric metering of wind-blown snow. *ANARE Interim Reports*. Ser. A(IV). Glaciology. Publication No. 79, p. 1–18.

Mellor, M. [1960.] Gauging Antarctic drift snow. (*In Antarctic meteorology. Proceedings of the symposium held in Melbourne, February 1959*. London, Pergamon Press, p. 347–55.)

Rogers, W. E. 1968. A photoelectric snow particle counter. *Transactions. American Geophysical Union*, Vol. 49, No. 4, p. 690. [Abstract.]

Schmidt, R. A. 1977. A system that measures blowing snow. *U.S. Dept. of Agriculture. Forest Service. Research Paper* RM-194.

Wishart, E. R. 1965. A new photoelectric drift snow gauge. *ANARE Interim Reports*. Ser. A(IV). Glaciology. Publication No. 79, p. 19–26.